ISSN 1027-5495. Functional Materials, 28, No.4 (2021), p. 669-675.
doi:https://doi.org/10.15407/fm28.04.669 © 2021 — STC "Institute for Single Crystals"

Effect of Zn doping on the structural and optical properties of NiO thin films deposited by spray pyrolysis technique

***A.Ferdi*[1,2], *A.Hafdallah*[1,3], *B.Harkati*[1,4], *L.Herissi*[1,5]**

[1]Department of Material Sciences, Faculty of SESNV, LarbiTebessi University-Tebessa, Algeria
[2]Laboratory of Study and Research of Condensed States, Badji Mokhtar-Annaba University, 23000 Annaba, Algeria
[3]Laboratory of Applied and Theoretical Physics(LPAT), Larbi Tebessi University-Tebessa, 12002 Tebessa, Algeria
[4]Laboratory of Bioactive Molecules and Applications, Larbi Tebessi University-Tebessa 12000, Algeria
[5]LMSSEF, Larbi ben M'Hidi University, 04000-Oum El Bouaghi, Algeria

Received May 11, 2021

We have prepared undoped and Zn-doped NiO thin films (2 wt. %, 4 wt. % and 6 wt. %) by spray pyrolysis technique, deposited on heated glass substrates (450°C). Nickel chloride hexahydrate and zinc acetate dihydrate have been used as starting precursors. The effect of zinc doping on the structural and optical properties of NiO thin films has been determined using X-ray diffraction and UV-visible spectroscopy, respectively. Structural analysis by X-ray diffraction confirmed that our samples are polycrystalline with cubic structure (FCC). The variations of the microstructural parameters such as the crystallite size, lattice constant and dislocation density in the films as a function of Zn doping concentration were investigated. The crystallite size increases gradually with an increase in the Zn doping degree. The values of the optical transmission and the optical band gap of the films decrease with an increase in the doping degree. The values of optical transmission of the films can reach from 45 % to 65 % in the visible range. The values of optical gap are varied between 3.62 eV and 3.69 eV.

Keywords: NiO, zinc doping, spray pyrolysis, XRD, optical band gap.

Вплив легування Zn на структурні та оптичні властивості тонких плівок NiO, осаджених методом розпилювального піролізу. *A.Ferdi, A.Hafdallah, B.Harkati, L.Herissi*

Досліджено нелеговані та леговані цинком тонкі плівки NiO (2 мас.%, 4 мас.% і 6 мас.%), отримані методом розпилювального піролізу, нанесені на нагріті скляні підкладки (450°C). Гексагідрат хлориду нікелю і дигідрат ацетату цинку використано в якості вихідних прекурсорів. Вплив легування цинком на структурні і оптичні властивості тонких плівок NiO визначено за допомогою рентгенівської дифракції та УФ видимої спектроскопії відповідно. Структурний аналіз методом дифракції рентгенівських променів підтвердив, що наші зразки є полікристалічними з кубічної структурою (ГЦК). Досліджено зміну мікроструктурних параметрів, таких як розмір кристалітів, постійна решітки та щільність дислокацій у плівках, в залежності від концентрації легування цинком. Розмір кристалітів поступово збільшується зі збільшенням ступеню легування Zn. Значення оптичного пропускання та оптичної ширини забороненої зони плівок зменшуються зі збільшенням ступеню легування. Оптичне пропускання плівок може досягати значень від 45 % до 65 % у видимому діапазоні. Значення оптичної щілини варіюються від 3,62 еВ до 3,69 еВ.

Исследованы нелегированные и легированные цинком тонкие пленки NiO (2 масс.%, 4 масс.% и 6 масс.%), полученные методом распылительного пиролиза, нанесенные на нагретые стеклянные подложки (450°C). Гексагидрат хлорида никеля и дигидрат ацетата цинка использованы в качестве исходных прекурсоров. Влияние легирования цинком на структурные и оптические свойства тонких пленок NiO определено с помощью рентгеновской дифракции и УФ-видимой спектроскопии соответственно. Структурный анализ методом дифракции рентгеновских лучей подтвердил, что наши образцы являются поликристаллическими с кубической структурой (ГЦК). Исследовано изменение микроструктурных параметров, таких как размер кристаллитов, постоянная решетки и плотность дислокаций в пленках, в зависимости от концентрации легирования цинком. Размер кристаллитов постепенно увеличивается с увеличением степени легирования Zn. Значения оптического пропускания и оптической ширины запрещенной зоны пленок уменьшаются с увеличением степени легирования. Оптическое пропускание пленок может достигать значений от 45 % до 65 % в видимом диапазоне. Значения оптической щели варьируются от 3,62 эВ до 3,69 эВ.

1. Introduction

Transparent conductive oxide (TCO) thin films are widely used in solar cells, light-emitting diodes, sensing and flat panel display devices [1]. Most of these TCOs are *n*-type semiconductors. However, thin films of *p*-type semiconductors are relatively rare but required in many applications. In 1997 Kawazoe et al. reported first *p*-type TCO in a highly transparent thin film of ($CuAlO_2$), which opened up a new field in transparent electronics applications [2–4]. Among them, nickel oxide (NiO) is one of the most exhaustively investigated *p*-type TCOs due to its low cost, non-toxicity, and high optical transparency. It is characterized by a wide band gap varying between 3.6 eV and 4.0 eV [5]. Generally, the variation of their physical properties is related to the change of deposition parameters such as precursor type, elaboration method, doping concentration, defects [6].

Stoichiometric NiO has a NaCl-like FCC structure [7]. However, Ni cation vacancies in NiO non-stoichiometric crystallites provide a wide variety in physical properties depending on the deposition process parameters and resulting defect structures. The presence of Ni^{2+} vacancy and/or interstitial oxygen creates Ni^{3+} ions in the NiO crystalline lattice following the reaction: $Ni^{2+} \rightarrow Ni^{3+} + e^-$ [7, 8].

Several experimental studies have been made to improve the physical properties of NiO thin films by doping with various chemical elements such as: Li [9], Co [10], Zn [11], etc. Zn is a promising transition metal element used for doping NiO due to its ionic radius which is close to that of Ni and it forms highly crystalline oxide materials [12].

Up to date, several methods have been used to prepare NiO thin films such as sputtering [13], pulsed laser deposition [14], evaporation [15], chemical bath deposition [16] and also spray pyrolysis [17, 18]. The latter is a simple and economical method for obtaining uniform NiO coatings over a large area due to the absence of a vacuum system and ease of setup. Moreover, it allows us to tune a lot of deposition parameters which plays a significant role in determining various properties of metal oxide thin films [4]. Due to these economically and experimentally favorable conditions, spray pyrolysis technique has been employed to prepare NiO thin films.

In this work, we have focused firstly on the deposition kinetic of Zn doped NiO thin films by spray pyrolysis technique and confirmation of the FCC structure. Second, the effect of Zn doping on structural and optical properties of resulting NiO thin films has been investigated. The obtained results provide valuable information about structural and optical properties of NiO, which is a very helpful issue for better understanding and perfection of the material quality for the electronic application.

2. Experimental

Zinc-doped nickel oxide thin films have been deposited onto heated glass substrates by spray pyrolysis (SP) technique. Before deposition, the substrates were first cleaned by acetone for eliminating any greasy track, then with methanol and at last abundantly rinsed with distilled water. Finally, they were dried. The substrate temperature during the deposition was fixed at 450°C. This temperature has been shown to be efficient to achieve NiO films [19]. Nickel chloride hexahydrate ($NiCl_2{\cdot}6H_2O$) and zinc acetate

Table 1. Optimized deposition parameters for the preparation of Zn-doped NiO thin films

Parameters	Values
Precursor	Nickel chloride hexahydrate
Dopant	Zinc acetate dihydrate
Solvent	Distilled water
Precursor concentration	0.1 M
Dopant concentration	0, 2, 4, 6 wt.%
Substrate temperature	450°C
Deposition time	5 min
Substrate-Nozzle distance	20 cm

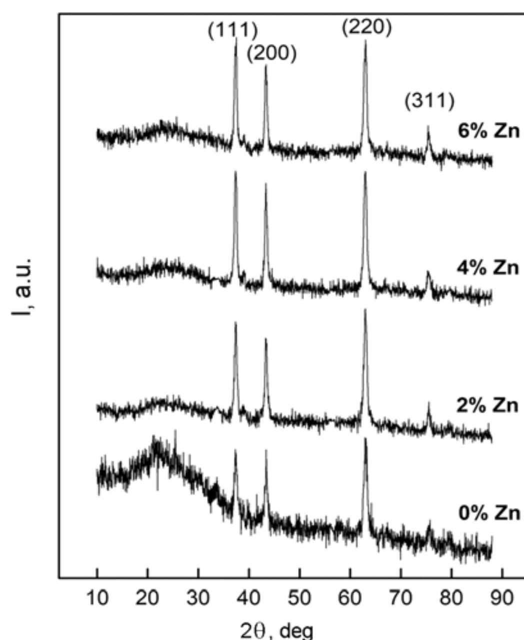

Fig. 1. XRD patterns of Zn-doped NiO thin films deposited by spray pyrolysis.

dihydrate ($Zn(C_2H_3O_2)_2 \cdot 2H_2O$) were used as precursor sources for NiO and Zn dopants respectively. 0.1 M of nickel chloride was dissolved in distilled water and Zn doping was achieved by addition of zinc acetate to the precursor solution. The doping weight concentrations (2, 4 and 6 wt.% Zn) have been measured by the weight percentile method using the molarity equation [20]. The resulting solution was stirred at room temperature for 20 min to yield a clear and homogeneous solution of green color. The deposition conditions for elaborated Zn doped NiO are listed in Table 1.

Spraying the solution on the surface of a heated substrate at a sufficient temperature makes it possible to decompose dissolved products in the solution (pyrolytic decomposition) and to activate the chemical reactions that can form a thin NiO film after the evaporation of excess elements. The reaction process can be expressed as the following:

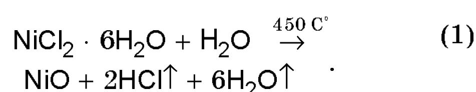

$$NiCl_2 \cdot 6H_2O + H_2O \xrightarrow{450\ C^\circ} NiO + 2HCl\uparrow + 6H_2O\uparrow \quad (1)$$

The film thickness has been estimated by Swanepoel's envelope method [21, 22]. The XRD patterns were measured by an X-ray diffractometer (Bruker-AXS, D8 advance) with CuKα radiation ($\lambda_{CuK\alpha}$ = 1.5418 Å). Transmittance spectra of the deposited films were measured in the range of 300–1100 nm using a SHUMADZU 1601 PC UV-visible spectrophotometer. All these measurements were performed at room temperature.

3. Results and discussion

3.1. Crystalline structure and orientations

The X-ray diffraction spectra of NiO thin films deposited on 450°C heated glass substrates and obtained at different zinc doping concentrations are shown in Fig. 1. The crystalline state of the thin films (crystalline or amorphous) can be determined from the XRD spectra. The XRD patterns show that our samples are polycrystalline. Indeed, the presence of various diffraction peaks [(111), (200), (220) and (311)] indicates that NiO films are polycrystalline with a cubic type crystal structure (FCC) as compared with the standard spectrum: JCPDS NiO card (JCPDS, N°04-0835). It can be mentioned that no diffraction peaks indicating the presence of other secondary phases were revealed in the XRD spectrum. As a rule, the positions of the peaks in the diffraction spectra of zinc-doped NiO films are slightly shifted towards a lower 2θ deg as compared to the undoped NiO film (Table 2). This shift results from the distor-

Table 2. Comparison of 2θ values of X-ray diffraction peaks (our samples) as a function of Zn doping concentration

Sample	2θ (111)	2θ (200)	2 θ (220)	2θ (311)
NiO:Zn (0 wt.%)	37.385	43.412	63.027	75.571
NiO:Zn (2 wt.%)	37.390	43.376	62.992	75.513
NiO:Zn (4 wt.%)	37.369	43.361	62.970	75.491
NiO:Zn (6 wt.%)	37.377	43.340	62.974	75.472
JCPDS NiO database	37.312	43.334	62.974	75.516

tion in the crystal lattice due to the introduction of the dopant Zn into the crystal lattice (ionic radii R (Zn^{+2}) = 74 pm and R (Ni^{+2}) = 69 pm) [23]). Moreover, the slight shift of peaks in the XRD spectra of pure NiO sample compared to the standard peaks position of JCPDS NiO can be attributed to the effect of the stress during the growth of our film.

3.2. Microstructural parameters

The lattice parameter a can be evaluated from the standard relation [24]:

$$d = \frac{a}{\sqrt{h^2 + k^2 + l^2}}. \quad (2)$$

Interplanar spacing d is calculated from Bragg's formula ($2d\sin\theta = n\lambda$) and (hkl) are the Miller indices of the planes.

The calculated values of the lattice parameter (a) and the unit cell volume (V) for each sample are given in Table 3. The crystalline structure of NiO is FCC and, therefore, the unit cell volume is calculated using the relation: $V = a^3$. The difference in the lattice parameter between undoped and Zn-doped NiO thin films is probably due to the substitution of the Ni^{+2} ions by Zn^{+2} doping ions of larger ionic radius as has been previously stated [23, 25]. This leads to a distortion of the lattice.

Table 3. Lattice constant and unit cell volume of NiO thin films as a function of Zn doping concentration ((JCPDS NiO database: a = 4.1769 Å).

Sample	a (111), Å	a (220), Å	V (111), Å^3	V (220), Å^3
Pure NiO (0 wt.%)	4.1629	4.1681	72.1419	72.4126
NiO:Zn (2 wt.%)	4.1623	4.1702	72.1107	72.5221
NiO:Zn (4 wt.%)	4.1646	4.1715	72.2303	72.5899
NiO:Zn (6 wt.%)	4.1637	4.1712	72.1835	72.5743

The crystallite size values (D) of the samples were estimated from Debye-Scherrer formula [26, 27] and their variations with different concentration of zinc doping are shown in Table 4.

$$D = \frac{0.9\lambda}{\beta\cos\theta}, \quad (3)$$

where β is the full width at half maximum (FWHM) of the diffraction peak in radian, λ is the X-ray wavelength ($\lambda_{CuK\alpha}$) and θ is the Bragg diffraction angle of the peak (in degrees).

The average crystallite size values (D_{av}) of NiO thin films (Fig. 2) were calculated from the peaks (111) and (220). We note that the crystallite size increases gradually with increasing of the doping rate (slight

Table 4. Values of full width at half maximum (FWHM) and crystallite size (D) for (111) and (220) planes of NiO thin films

Sample	(111) peak Position (°) (2Θ)	(111) peak Intensity (a.u.)	FWHM (111) peak (°)	D (111) (nm)	(220) peak Position (°) (2Θ)	(220) peak Intensity (a.u.)	FWHM (220) peak (°)	D (220) (nm)
NiO:Zn (0 wt.%)	37.385	299.306	0.5258	16.66	63.027	251.897	0.6683	14.57
NiO:Zn (2 wt.%)	37.390	195.311	0.5003	17.51	62.992	172.107	0.5907	16.48
NiO:Zn (4 wt.%)	37.369	209.824	0.4716	18.58	62.970	192.983	0.5702	17.07
NiO:Zn (6 wt.%)	37.377	228.144	0.4723	18.55	62.974	206.597	0.5749	16.93

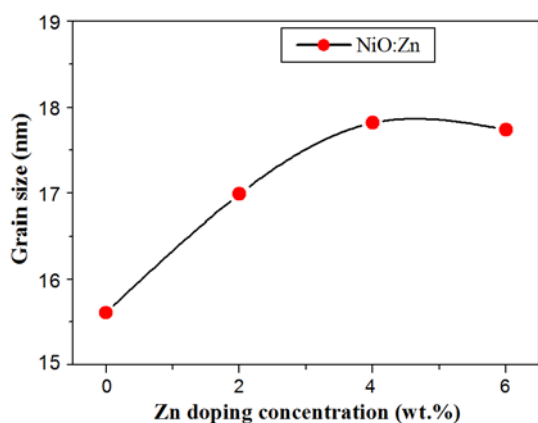

Fig. 2. Variations of the average crystallite size of pure NiO and Zn-doped NiO thin films at different concentrations of Zn.

increase). The same result has been obtained by other authors [25].

The thickness of the films varied from 332 nm to 354 nm depending on the doping concentration. The number of crystallites per unit area (N) and the dislocation density (δ) [28, 29] in the films have been determined by the following relations, and their values are given in Table 5.

$$N = \frac{t}{D_{av}^3}, \quad (4)$$

$$\delta = \frac{1}{D_{av}^2}. \quad (5)$$

Here t is the film thickness and D_{av} is the average crystallite size.

3.3. Optical properties

The dependence of the optical transmission on the wavelength (λ) in the spectral range of 300–1100 nm for NiO and Zn-doped NiO films prepared at different Zn doping rates is shown in Fig. 3. The general appearance of the transmission spectra is identical. All of these spectra are composed of two regions:

— A region of high absorption corresponds to the fundamental absorption ($\lambda < 400$ nm). This absorption is due to the interband electronic transition (between the valence band and the conduction band). The size of the optical gap is determined by the change in transmission in this region.

— A second region of high transparency is located between 400 and 1100 nm. It can be seen that the transmission is decreased with an increase in the dopant concentration. Indeed, the dopant atoms (Zn) intro-

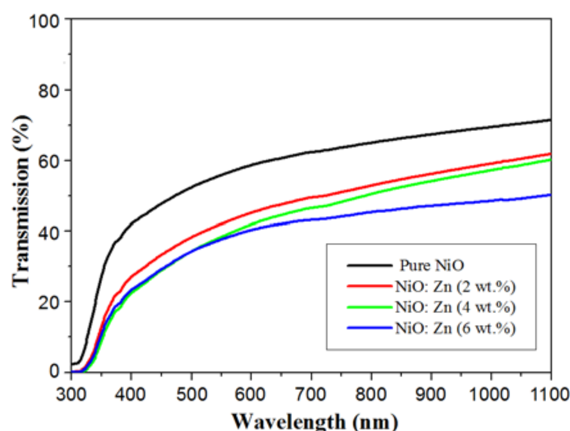

Fig. 3. Transmission spectra of Zn-doped NiO thin films.

Table 5.The number of crystallites per unit area and the dislocation density in NiO:Zn thin films

Sample	Number of crystallites per unit area (N): 10^{12} cm^{-2}	Dislocation density (δ): 10^{11} lines/cm^2
Pure NiO	9.201	4.103
NiO:Zn (2 wt.%)	6.769	3.464
NiO:Zn (4 wt.%)	6.255	3.149
NiO:Zn (6 wt.%)	6.197	3.177

duced into the crystal lattice of NiO films take the substitutional sites ($R(Zn^{2+}) \approx R(Ni^{2+})$). The decrease in the transmittance with an increase in the concentration of dopant Zn atoms is explained by increasing disorder in thin films (Fig. 4). The transmittance of pure NiO thin film is nearly 65 % and it decreases to 45 % at 6 % Zn in the visible region. This behavior was observed by other authors [11, 30].

3.4. Study of the disorder (Urbach energy)

The Urbach relation was used to determine the state of disorder in our samples from the change in the absorption coefficient. The absorption coefficient (α) is related with the Urbach energy (E_u) by the expression [31]:

$$\alpha = \alpha_0 \exp(h\nu / E_u) \quad (6)$$

where α_0 is a constant.

The value of E_u, which characterizes the disorder, can be obtained from the dependence $\ln\alpha$ as a function of $h\nu$ and its straight-line slope. Fig. 4 shows the variation of disorder in NiO thin films as a function of Zn concentration. From this fig-

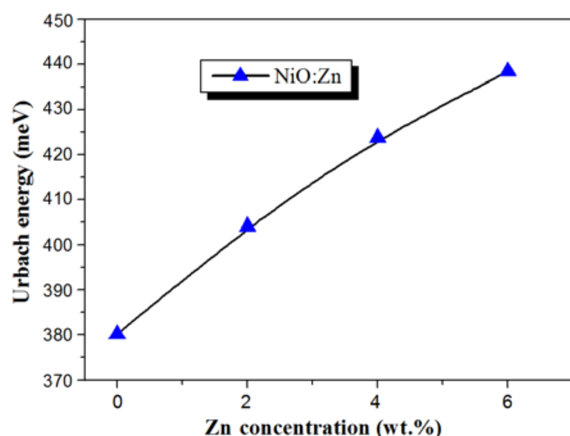

Fig. 4. Variation of the Urbach energy in NiO films as a function of Zn concentration.

ure it can be seen that the degree of disorder increases with increasing zinc dopant. This can be attributed to a decrease in the crystalline order in our films with increasing the value of incorporated foreign atoms (Zn) in the NiO lattice (creation of defects).

3.5. Optical band gap

The NiO material has a direct band gap; in this case, the absorption coefficient (α) as a function of the optical band gap (E_g) is expressed by the Tauc relation [8, 32]:

$$\alpha h\nu = A(h\nu - E_g)^{1/2}. \quad (7)$$

Here A is a constant; E_g is the optical energy gap expressed in eV; $h\nu$ is the photon energy.

We can determine the value of the optical energy gap (E_g) by the extrapolation of the straight-line portion of the spectrum $(\alpha h\nu)^2 = f(h\nu)$ to the zero value of the energy axis. The variations of the optical energy gap values for our films are shown in Fig. 5. The optical band gap of NiO:Zn films slightly decreases from 3.69 eV to 3.62 eV with increasing Zn concentration. This can be explained by a higher mobility of free electrons due to the effect of the dopant atoms (Zn^{2+}), since the mobility of charge carriers in ZnO is greater than that in NiO [33–36]. The slight difference in the variation of the gap is explained by the fact that the doping element (Zn) has two valence electrons (Zn^{2+}) like Ni; and their atomic radii are $R(Zn^{2+}) \approx R(Ni^{2+})$. The same results on the decrease in E_g was reported by R.Sharma et al. [11] for Zn-doped NiO thin films deposited by spray pyrolysis, or by other techniques [25, 30].

In Fig. 6 we have reported a comparison between the variation of the band gap energy (E_g) and that of the Urbach energy (E_u) as a function of Zn concentration. A decrease in E_g with increasing E_u is due to an increased Zn doping (substitutional atoms) in the crystal lattice of NiO films which leads to the decrease in E_g values as has been explained previously.

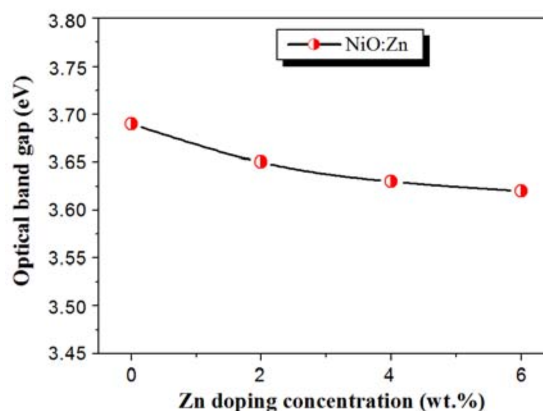

Fig. 5. Variation of the optical band gap energy of NiO thin films as a function of Zn dopant concentration.

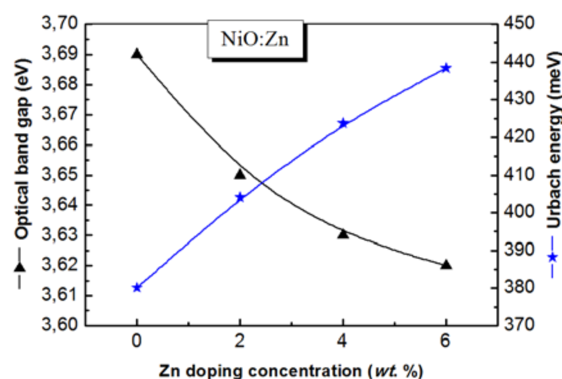

Fig. 6. Variation of the optical band gap energy and Urbach energy as a function of Zn dopant concentration.

4. Conclusions

Thus we studied the influence of Zn doping degree (2 wt.%, 4 wt.% and 6 wt.%) on the evolution of structural and optical properties of NiO thin films synthesized by spray pyrolysis. These films (undoped and Zn-doped NiO) were deposited on heated glass substrates (450°C) with a concentration of 0.1 mol/l. With regard to the structural properties of the films, the XRD results confirmed that our samples are polycrystalline with FCC structure. The difference in the lattice constant between undoped and Zn-doped NiO thin films is probably due to the substitution of the Ni^{2+} ions by Zn^{2+} doping ions with a larger ionic

radius. The average crystallite size increases gradually with increasing Zn concentration. From the study of optical properties, the transmission decreases with increasing Zn concentration due to an increase in the dopant concentration (distortion in the crystal lattice). This behavior is explained by increasing the disorder in the thin films. The optical band gap of our films slightly decreases with increasing dopant concentration. This can be explained by the higher mobility of free electrons due to the effect of the dopant atoms (Zn^{2+}) since the mobility of charge carriers in ZnO is greater than that in NiO. The values of E_g of the films vary between 3.62 eV and 3.69 eV.

References

1. Y.Li, R.Yao, H.Wang et al., *ACS Appl. Mater. Inter.*, **9**, 11711 (2017).
2. H.Kawazoe, M.Yasukawa, H.Hyodo et al., *Nature*, **389**, 939 (1997).
3. G.Thomas, *Nature*, **389**, 907 (1997).
4. M.M.Gomaa, G.R.Yazdi, S.Schmidt et al., *Mater. Sci. Semicon. Proc.*, **64**, 32 (2017).
5. Z.T.Khodair, B.A.Ibrahim, M.K.Hassan, *Mater. Today*, **20**, 560 (2020).
6. T.Chtouki, L.Soumahoro, B.Kulyk et al., *Optik*, **128**, 8 (2017).
7. R.Sharma, A.D.Acharya, S.B.Shrivastava et al., *Optik*, **125**, 6751 (2014).
8. B.Subramanian, M.M.Ibrahim, V.Senthilkumar et al., *Physica B*, **403**, 4104 (2008).
9. C.C.Wu, C.F.Yang, *Nanoscale. Res. Lett.*, **8**, 33 (2013).
10. A.Dihaa, S.Benramache, B.Benhaoua, *Optik-Int. J. Light Elect. Optics*, **172**, 832 (2018).
11. R.Sharma, A.D.Acharya, S.B.Shrivastava et al., *Optik — Int. J. Light Elect. Optics*, **127**, 4661 (2016).
12. J.H.Lee, Y.W.Noh, I.S.Jin, J.W.Jung, *Electrochim. Acta*, **284**, 253 (2018).
13. S.C.Chen,T.Y.Kuo, H.C.Lin et al., *Appl. Surf. Sci*, **508**, 145106 (2020).
14. D.Singh, A.Das, R.S.Ajimsha et al., *Mater. Sci. Semicon. Proc.*, **66**, 186 (2017).
15. W.Li, X.Zhang, X.Chen et al., *Mater. Lett.*, **265**, 127464 (2020).
16. M.R.Das, A.Mukherjee, P.Mitra, *Physica E*, **93**, 243 (2017).
17. K.Sajilal, A.M.E.Raj, *Mater. Lett.*, **164**, 547 (2016).
18. S.R.Ardekani, A.S.R.Aghdam, M.Nazari et al., *J. Anal. Appl. Pyrol.*, **141**, 104631 (2019).
19. L.Cattin, B.A.Reguig, A.Khelil et al., *Appl. Surf. Sci.*, **254**, 5814 (2008).
20. A.D.Acharya, S.Moghe, R.Panda et al., *Thin Solid Films*, **525**, 55 (2012).
21. R.Swanepoel, *J. Phys. E: Sci. Instrum.*, **16**, 1214 (1983)
22. E.R.Shaaban, I.S.Yahia, E.G.El-Metwally, *Acta. Phys. Pol A.*, **121**, 628 (2012).
23. C.Thangamani, K.Pushpanathan, *J. Chem. Pharm. Res.*, **8**, 749 (2016).
24. Y.M.Lu, W.S.Hwang, J.S.Yang, H.C.Chuang, *Thin Solid Films*, **420–421**, 54 (2002).
25. F.S.Hashim, N.A.Sami, *Int. Lett. Chem. Phys. Astr.*, **53**, 31 (2015).
26. S.Benramache, B.Benhaoua, *Superlattice. Microst.*, **52**, 807 (2012).
27. H.Wanga, D.Mishra, P.Chen, J.Ting, *J. Alloy. Compd.*, **584**, 142 (2014).
28. T.Mahalingam, V.Dhanasekaran, R.Chandramohan, J.K.Rhee, *J. Mater. Sci.*, **47**, 1950 (2012).
29. S.Prabahar, M.Dhanam, *J. Cryst. Growth.* **285** 41 (2005).
30. I.Manouchehri, S.A.O.Alshiaa, D.Mehrparparvar et al., *Optik*, **127**, 9400 (2016).
31. F.Ynineb, A.Hafdallah, M.S.Aida et al., *Mater. Sci. Semicon. Proc.*, **16**, 2021 (2013).
32. S.Benhamida, B.Benhaoua, R.Barir et al., *J. Nano-Elec. Phys.*, **9**, 03004 (2017).
33. H.Sato, T.Minami, S.Takata, T.Yamada, *Thin Solid Films*, **236**, 27 (1993).
34. Y.Igasaki, H.Saito, *J. Appl. Phys.*, **69**, 2190 (1991).
35. W.S.Lau, S.J.Fonash, *J. Electron.Mater.*, **16**, 141 (1987).
36. J.D.Merchant, M.Cocivera, *Chem. Mater.*, **7**, 1742 (1995).